


Article

New Construction of Functionalized CuO/Al₂O₃ Nanocomposite-Based Polymeric Sensor for Potentiometric Estimation of Naltrexone Hydrochloride in Commercial Formulations

Amal M. Al-Mohaimeed ¹, Gamal A. E. Mostafa ^{2,*} and Maha F. El-Tohamy ^{1,*}

¹ Department of Chemistry, College of Science, King Saud University, P.O. Box 22452, Riyadh 11451, Saudi Arabia; muhemeed@ksu.edu.sa

² Department of Pharmaceutical Chemistry, College of Pharmacy, King Saud University, P.O. Box 2457, Riyadh 11451, Saudi Arabia

* Correspondence: gmostafa@ksu.edu.sa (G.A.E.M.); moraby@ksu.edu.sa (M.F.E.-T.)

Abstract: Electrically conductive polymeric nanocomposites with nanoparticles are adaptable types of nanomaterials that are prospective for various applications. The extraordinary features of copper oxide (CuO) and aluminium oxide (Al₂O₃) nanostructures, encourages extensive studies to prospect these metal oxide nanocomposites as potential electroactive materials in sensing and biosensing applications. This study suggested a new CuO/Al₂O₃ nanocomposite-based polymeric coated wire membrane sensor for estimating naltrexone hydrochloride (NTX) in commercial formulations. Naltrexone hydrochloride and sodium tetraphenylborate (Na-TPB) were incorporated in the presence of polymeric polyvinyl chloride (PVC) and solvent mediator *o*-nitrophenyloctyl ether (*o*-NPOE) to form naltrexone tetraphenylborate (NTX-TPB) as an electroactive material. The modified sensor using NTX-TPB-CuO/Al₂O₃ nanocomposite displayed high selectivity and sensitivity for the discrimination and quantification of NTX with a linearity range 1.0×10^{-9} – 1.0×10^{-2} mol L⁻¹ and a regression equation $E_{mV} = (58.25 \pm 0.3) \log [\text{NTX}] + 754.25$. Contrarily, the unmodified coated wire sensor of NTX-TPB exhibited a Nernstian response at 1.0×10^{-5} – 1.0×10^{-2} mol L⁻¹ and a regression equation $E_{mV} = (52.1 \pm 0.2) \log [\text{NTX}] + 406.6$. The suggested modified potentiometric system was validated with respect to various criteria using the methodology recommended guidelines.

Keywords: naltrexone hydrochloride; nanocomposites; polymeric sensors; commercial formulations



Citation: Al-Mohaimeed, A.M.; Mostafa, G.A.E.; El-Tohamy, M.F. New Construction of Functionalized CuO/Al₂O₃ Nanocomposite-Based Polymeric Sensor for Potentiometric Estimation of Naltrexone Hydrochloride in Commercial Formulations. *Polymers* **2021**, *13*, 4459. <https://doi.org/10.3390/polym13244459>

Academic Editor: Dong Jin Yoo

Received: 30 November 2021

Accepted: 17 December 2021

Published: 20 December 2021

Publisher's Note: MDPI stays neutral with regard to jurisdictional claims in published maps and institutional affiliations.



Copyright: © 2021 by the authors. Licensee MDPI, Basel, Switzerland. This article is an open access article distributed under the terms and conditions of the Creative Commons Attribution (CC BY) license (<https://creativecommons.org/licenses/by/4.0/>).

1. Introduction

Advances in nanoscience technologies and nanomaterial engineering have opened up new areas in scientific research and the evolution of modified sensing and biosensing probes. The current studies have focused on the production of nanocomposites instead of single nanoparticles. These nanocomposites usually possess different nanoscale domains, which induce synergistic effects as a result of their interfacial interactions [1].

Nanocomposites hold both extraordinary characteristics of nanomaterials and polymer advantages including, chemical resistance, high conductivity, biocompatibility and elasticity [2]. The recent progress in scientific areas, such as chemical engineering [3], biochemistry [4] and physics [5], require the development of novel sensing technologies that combine lower power utilization and miniaturization with highly tactile sensitivity. Nanocomposites are also nanostructures with high activities that exhibit unusual significant combinations and unique engineering possibilities. With increasing the growth rate and rapid inquire to be in sensor constructions, their potential is so prominent that they are successfully utilized in various sensing and biosensing applications [6]. They have appeared as viable alternatives to control the drawbacks of micro composites. Furthermore, these materials are having extraordinary designs and unique optical characteristics that

are not present in conventional composites [7]. Additionally, the nanocomposite synthesis is considered to be the main step in construction of various electronic devices [8], drug delivery systems [9], biomedical and immunosensing applications [10,11].

Currently, several reports are focused on metal oxides, including aluminium oxide (Al_2O_3), copper oxide (CuO), nickel oxide (NiO), etc. Moreover, more attention has been focused on the perspective of copper oxide in various aspects such as antibacterial agents [12], catalysis [13], food packaging [14], sensors [15] and medicine [16]. Recently, there has been a growing awareness of the development of aluminium oxide nanoparticles (Al_2O_3 NPs) which have a high specific surface area with extraordinary optical, catalytic, thermodynamic stability properties for progressive engineering and industrial applications [17–19]. Few studies reported the use of CuO/ Al_2O_3 in sensing applications such as Khan et al. [20] studied the electrochemical oxidation of ammonia over copper oxide impregnated γ - Al_2O_3 nanocatalysts. Also, the structural features, electrical characteristics and gas sensing applications of polymeric copper/alumina hybrid nanocomposite has been reported by Sankar et al. [21]. Another study conducted by using the p-Type copper aluminium oxide thin films for gas-sensing applications has been reported by Baratto et al. [22].

Some recent studies reported the synthesis of CuONPs and Al_2O_3 NPs by various techniques, including pyrolysis, sol-gel, sputtering, laser ablation and electrochemical reduction [23–32]. Sodeifian and Behnood [33] reported a microwave-assisted method for the synthesis of CuO/ Al_2O_3 nanocomposite for photocatalytic degradation of methylene blue removal from aqueous solution under UV irradiation.

Electrochemical techniques, including amperometry, conductometry and potentiometry are more reliable and economical techniques suitable for in-field of sensing, biosensing, chemical analysis and biomedical applications [34–37]. These techniques are also fast in terms of spending short analytical time, allowing on-line detecting of aqueous samples. The potentiometric technique is one of the most promising self-powered techniques in which the potential difference measurements are resulted from the accumulation of analytes under the electrostatic mechanism on the surface of the working electrode and the reference one [38]. Recently, various potentiometric sensors have been modified with metal, metal oxides and nanocomposites or coupled with biosensing electrodes to enhance their sensitivity and limits of detection [39,40]. Various dozens of compounds can be estimated with the potentiometric sensors that commonly contain membranes fabricated from high molecular weight polyvinyl chloride (PVC), plasticizers, including dioctyl sebacate (DOS), dioctyl phthalate (DOP), dibutyl sebacate (DBS), dibutyl phthalate (DBP) and *o*-nitrophenyl octyl ether (*o*-NPOE) as solvent mediator. Additionally, these membranes also formed from lipophilic ions or molecules, acting as active materials to produce specific analyte interaction in the membrane sites for pre-detection of the selectivity of the relating sensors [41].

The potentiometric coated wire sensors are commonly constructed from highly conductive metal wire such as silver, gold, platinum, copper and aluminium. The metal wire is used as a substrate which is coated with a polymeric cocktail containing the active sites of the selective membrane [42]. Sodium tetraphenylborate (Na-TPB) is a white powder that has the ability to catalyze the ion-exchange process via the interfaces of hydrophobic membrane when used with a suitable ion-pair complex [43].

Naltrexone hydrochloride (NTX), is an opioid medication antagonist, primarily used to control opioid and alcohol disorders (Figure 1). It has also been found to have potential in the case of euphoria associated with drug abuse disorders [44]. NTX was previously estimated and quantified by several analytical techniques, such as spectroscopic [45], chromatographic separation [46,47], and electrochemical methods [48]. Although these previously reported techniques exhibited acceptable sensitivity and selectivity for NTX detection, they still have certain limitations as they require long analytical separation time, high technical skills and consumption of large amounts of solvents.

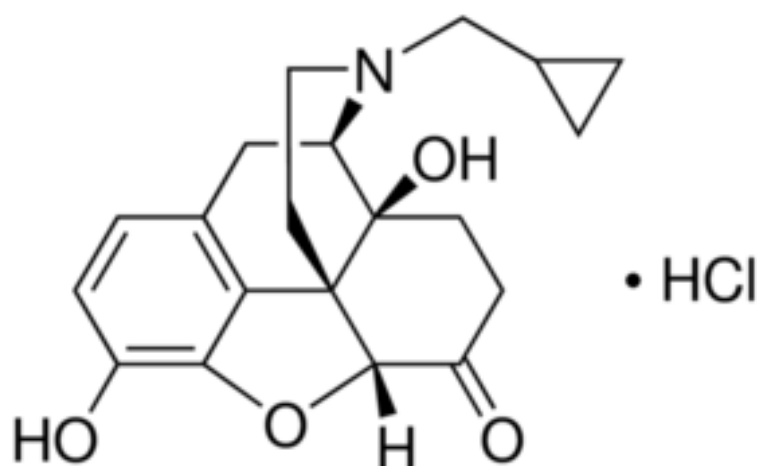


Figure 1. Structural formula of Naltrexone hydrochloride.

The objective of this study was to design a modified metal oxide ($\text{CuO}/\text{Al}_2\text{O}_3$) nanocomposite coated wire sensor with ultra-sensitivity and selectivity towards the detection of NLX in its commercial products. A new strategy involving exploiting the unique physical, chemical, optical and conductive properties of the selected metal oxides has been suggested to enhance the sensitivity and selectivity of the potentiometric modified sensor. The incorporation of $\text{CuO}/\text{Al}_2\text{O}_3$ in polymeric matrix will play an impact role in the sensitivity and selectivity of the suggested sensor towards the determined drug. To ensure the analytical suitability of the suggested method, method validation is according to ICH guidelines [49]. Furthermore, a comparative study was carried out between the suggested $\text{CuO}/\text{Al}_2\text{O}_3$ nanocomposite coated membrane sensor and the conventionally designed type.

2. Materials and methods

2.1. Chemicals

Pure grade of opioid antagonist medication Naltrexone hydrochloride and Naltrexone hydrochloride[®] tablets (50 mg/tablet) was gained from (Intas Pharmaceuticals Limited, Ahmedabad, India). Sigma Aldrich, Hamburg, Germany, supplied various analytical chemicals and solvents, including acetone 99.9%, methanol 99.9%, ethanol 99.9%, tetrahydrofuran (THF) 97.0%, *o*-NPOE, hydrochloric acid 37%, sodium tetraphenylborate (Na-TPB) and high molecular weight PVC. Copper chloride (99.0%), aluminium nitrate nonahydrate (99.9%) and sodium hydroxide (99.9%) were obtained from BDH (Poole, UK).

2.2. Instruments

This study was conducted using a “digital pH meter HANNA, model 211 (HANNA instruments, Rhode Island, Woonsocket, RI, United States) and the pH meter Metrohm pH-meter model 744 (Metrohm Co., Herisau, Switzerland) was used to adjust the pH of the sample solution throughout the experiments. The designed potentiometric system was consisted of a constructed conventional naltrexone hydrochloride-tetraphenyl borate (NTX-TPB) or modified NTX-TPB- $\text{CuO}/\text{Al}_2\text{O}_3$ nanocomposite coated wire sensor in conjunction with silver/silver chloride (Ag/AgCl) as reference one. The synthesized metal oxide nanoparticles and the nanocomposite were characterized using various spectroscopic and microscopic techniques, including UV-2450 spectrophotometer (Shimadzu Corporation, Kyoto, Japan), Fourier-Transform Infrared spectroscopy (FT-IR) Spectrum BX spectrometer (PerkinElmer, Waltham, Massachusetts, United States). X-ray diffraction (XRD) Shimadzu XRD-6000 diffractometer (Shimadzu, Kyoto, Japan), scanning electron microscope (SEM) JSM-7610F (JEOL Ltd., Tokyo, Japan), and a transmission electron microscope (TEM) JEM-2100F, (JEOL Ltd., Tokyo, Japan). Furthermore, Energy-Dispersive X-ray Spectroscopy

(EDX), using EDX-8100 (Shimadzu, Kyoto, Japan) analysis was applied to detect the presence of Cu, Al and O elements in the synthesized nanomaterials.

2.3. Preparation of NTX-TPB Electroactive Complex

The electroactive compound NTX-TPB was prepared by mixing equal volume (50 mL) of an equimolar concentration ($1.0 \times 10^{-2} \text{ mol L}^{-1}$) of aqueous NTX and TPB solution. A white precipitate of NTX-TPB was formed. The mixture solution was filtered using Whatman filter paper No. 41 and the precipitate was washed using deionized water and left to dry overnight.

2.4. Synthesis of CuO and Al₂O₃ Nanoparticles

The precipitation method was used to synthesize CuO nanoparticles by dissolving 1.596 g of copper nitrate ($\text{Cu}(\text{NO}_3)_2 \cdot 3\text{H}_2\text{O}$) in 100 mL deionized water to form 0.1 mol L^{-1} concentration. An aqueous sodium hydroxide solution (0.1 mol L^{-1}) was prepared and slowly added dropwise under vigorous stirring until the pH achieved 14. The formed precipitate was repeatedly washed three times and neutralized by deionized water and absolute ethanol. Subsequently, the resulting precipitate was dried at $80 \text{ }^\circ\text{C}$ for 12 h, then it was calcined for 4 h at $500 \text{ }^\circ\text{C}$.

Al₂O₃ nanoparticles were prepared using a sol-gel method by heating a solution of citric acid/aluminium nitrate nonahydrate prepared in deionized water with a molar ratio of 0.5. The solution was heated at $60 \text{ }^\circ\text{C}$ under continuous stirring until the formation of white sol. The resulted gel was heated under constant stirring up to $80 \text{ }^\circ\text{C}$ until the formation of transparent gel. The formed gel was dried in an oven for 12 h at $90 \text{ }^\circ\text{C}$ and then ground and sintered at $600 \text{ }^\circ\text{C}$ for 4 h.

2.5. Synthesis of Polymeric NTX-TPB-CuO/Al₂O₃ Nanocomposite

The polymeric solution of CuO/Al₂O₃ nanocomposite was prepared by dissolving 5 mg of each previously prepared CuO and Al₂O₃ nanoparticles, 10 mg NTX-TPB ion pair, 190 mg of PVC and 0.35 mL *o*-nitrophenyloctyl ether in 5 mL THF under continuous stirring to form a polymeric cocktail of NTX-TPB-CuO/Al₂O₃ nanocomposite. Then, it was used to modify the surface of the suggested modified NTX-TPB-CuO/Al₂O₃ nanocomposite sensor.

2.6. Characterization of Synthesized Nanomaterials

Spectroscopic analysis for the synthesized CuO, Al₂O₃ and CuO/Al₂O₃ nanomaterials was performed at a wavelength range of 200–500 nm to confirm their formation. FT-IR detection was also conducted to determine the possible functional groups that can appear in the CuO, Al₂O₃ and CuO/Al₂O₃ nanomaterials spectra. Further investigation was carried out by XRD analysis using $\text{K}\alpha$ radiation ($\lambda = 1.5418 \text{ \AA}$) under 40 kV voltage and an operating current of 35 mA. The results of XRD were estimated at ambient temperature using a scan rate of 0.3 s/point and 0.02° resolution. The morphological shape and size distribution were studied using scanning and transmission electron microscope.

2.7. Preparation of Standard NTX Solution

The standard NTX ($1.0 \times 10^{-2} \text{ mol L}^{-1}$) solution was prepared by dissolving 0.341 g of pure NTX powder in 100 mL deionized water. The different working analytical solutions were prepared by serial dilution in water.

2.8. Sensor Construction and Membrane Composition

A conventional (NTX-TPB) coated wire sensor was constructed using a mixture of (PVC, 190 mg), electroactive material (NTX-TPB, 10 mg) and plasticizer (*o*-NPOE, 0.35 mL) in 5 mL of THF. The resulted polymeric mixture was poured into a Petri dish and kept at room temperature to evaporate slowly. The tip of the aluminium wire was polished and cleaned using deionized water, followed by acetone. The tip of the cleaned wire was

immersed several times in the polymeric membrane solution (NTX-TPB) until the formation of coated membrane on its surface. To construct the modified sensor another clean Al wire was dipped three times in the polymeric solution of CuO/Al₂O₃ nanocomposite to produce a thin layer membrane on its surface. The sensor was allowed to dry, then dipped again in the above polymeric (NTX-TPB) solution several times until the formation of a uniform coated membrane. Both coated wire sensors were assembled as Al wire/coated membrane/test solution//Ag/AgCl reference electrode. Figure 2 demonstrated the preparation of the designed modified NTX-TPB-CuO/Al₂O₃ nanocomposite sensor and the potentiometric system.

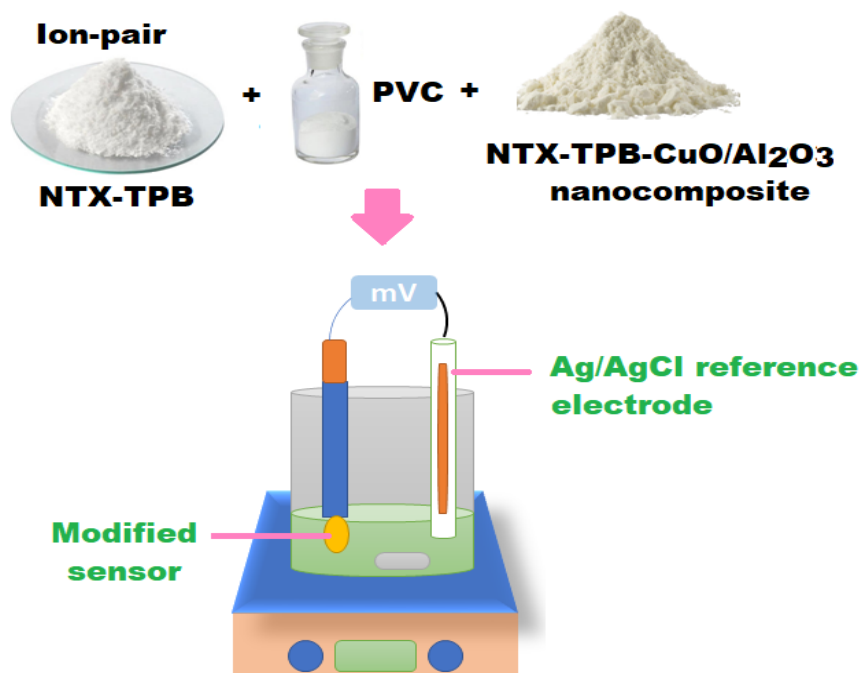


Figure 2. Schematic illustration for the preparation of the designed modified NTX-TPB-CuO/Al₂O₃ nanocomposite sensor and the potentiometric system.

2.9. Calibration Graphs

The linear relationship between the -logarithm NTX concentrations (mol L⁻¹) and the potential difference (mV) of each conventional (NTX-TPB) and modified (NTX-TPB-CuO/Al₂O₃) nanocomposite was determined. The calibration graphs were plotted using 50 mL of NTX standard solutions in the concentration range 1.0×10^{-9} – 1.0×10^{-2} mol L⁻¹ using the constructed working NTX-TPB or NTX-TPB-CuO/Al₂O₃ nanocomposite sensors separately in connection with a reference electrode (Ag/AgCl). The surface of the sensor should be cleaned with deionized water and dried with tissue paper prior to every measurement.

2.10. Optimization of Analytical Conditions

The potential response of the constructed coated wire sensors can be significantly affected by the change in the pH of the investigated solutions. The suitable pH range of conventional NTX-TPB and modified NTX-TPB-CuO/Al₂O₃ nanocomposite sensors was determined using 1.0×10^{-4} mol L⁻¹ NTX solution. The pH of the tested sample was acidified using 0.1 mol L⁻¹ of hydrochloric acid. The potential response of the working sensor was measured after increasing the pH value using 0.1 mol L⁻¹ sodium hydroxide solution. The pH graphs were constructed using the change in potential against the pH.

A separate solution method [50] was used to monitor the selectivity of the investigated NTX sensors. Briefly, the selectivity coefficient of each sensor towards NTX and some foreign substances and additives such as (Povidone, hydroxypropyl methylcellulose,

lactose monohydrate, magnesium stearate, microcrystalline cellulose, polyethylene glycol, polysorbate 80, tryptophan, lysine, and glycine) was determined using 1.0×10^{-3} mol L⁻¹ of NTX solution. The selectivity coefficient of conventional NTX-TPB and modified NTX-TPB-CuO/Al₂O₃ nanocomposite was calculated using the following equation:

$$\text{Log } K^{\text{Pot}} = (E_2 - E_1)/S + \log [\text{Drug}] - \text{Log } [B^{z+}]^{1/z} \quad (1)$$

where K^{Pot} (selectivity coefficient), E_1 (electrode potential) of 1.0×10^{-3} mol L⁻¹ NTX, E_2 (electrode potential) of 1.0×10^{-3} mol L⁻¹ of interfering species, B^{z+} (interfering species), and S (slope) of the calibration curve, respectively. The response time was tested by recording the dynamic potential response of the investigated drug, using NTX concentration range of 1.0×10^{-9} – 1.0×10^{-2} mol L⁻¹.

2.11. Estimation of Naltrexone Hydrochloride[®] Tablets

The content of ten naltrexone hydrochloride[®] tablets (50 mg/tablet) was pulverized and mixed well. An accurate quantity of 0.341 g was dissolved in 50 mL deionized water, then centrifuged at 1500 rpm for 5 min and filtered to remove the co-additive materials. The clear solution was completed with deionized water to be 100 mL, the resulting NTX solution (1.0×10^{-2} mol L⁻¹) was diluted with the same solvent to prepare the working analytical samples in the range of 1.0×10^{-5} – 1.0×10^{-2} and 1.0×10^{-9} – 1.0×10^{-2} mol L⁻¹. The designed NTX-TPB and modified NTX-TPB-CuO/Al₂O₃ nanocomposite sensors were separately utilized to quantify the investigated drug in its commercial tablets.

3. Results and Discussion

3.1. Characterization of CuO/Al₂O₃ Nanocomposite

Various spectroscopic techniques such as UV-Vis, FT-IR, XRD, and EDS were exploited to characterize the synthesized CuONPs/Al₂O₃NPs nanocomposite. One of the most suitable and useful methods for primary confirmation of shape, size and stability of the engineered nanoparticles in their aqueous suspensions is the UV-Vis method. The recorded spectrum of CuONPs/Al₂O₃NPs displayed two significant broad absorption peaks at 280 and 400 nm for CuO and Al₂O₃ nanoparticles, respectively (Figure 3). The band gaps of the as-synthesized metal oxide nanoparticles were calculated from the formula:

$$E_g = h\nu = hc/\lambda \quad (2)$$

where “ h ” is Planck’s constant, c is the velocity of light, and λ is the wavelength.” The optical band gap energy of CuONPs and Al₂O₃NPs were estimated to be 2.85 eV and 3.54 eV, respectively [51,52].

The FT-IR spectra of the pre-synthesized CuONPs, Al₂O₃NPs, and CuO/Al₂O₃ nanocomposite were performed in the range in range of 400–4000 cm⁻¹. The FT-IR spectrum of CuONPs (Figure 4a) showed different absorption bands at 3424.25 cm⁻¹ (O-H stretching vibration), 1632.22 cm⁻¹ (O-H bending vibration of absorbed water), 1466.58 cm⁻¹ and 1112.15 cm⁻¹ (CO₂ of the surrounding atmosphere), and 590 cm⁻¹ and 511 cm⁻¹ (Cu-O stretching bond formation). The obtained results are in agreement with those previously reported [53]. Figure 4b, described the FT-IR spectrum of Al₂O₃NPs. Broad and weak absorption bands appeared at 3499.11 cm⁻¹ and 1644.25 cm⁻¹ were due to stretching and bending O-H vibration of absorbed water, respectively; the band observed at 1369.12 cm⁻¹ was corresponding to stretching vibration of Al-OH bond, 1087.00 cm⁻¹ assigned to be corresponding to strong C-O stretching vibration. The peaks at 846.14 cm⁻¹ and 607.15 cm⁻¹ correspond to the Al-O bond [52]. In the CuO/Al₂O₃ nanocomposite FT-IR spectrum, different absorption vibration peaks were recorded at 3432.42 cm⁻¹ (O-H stretching vibration), 2353.69 cm⁻¹ (O=C=O of the surrounding atmosphere and 1633.56 cm⁻¹ (O-H vibration mode of water). The appearance of two stretching vibration peaks at 520.15 and 608.14 cm⁻¹ indicated the formation of CuO/Al₂O₃ nanocomposite (Figure 4c).

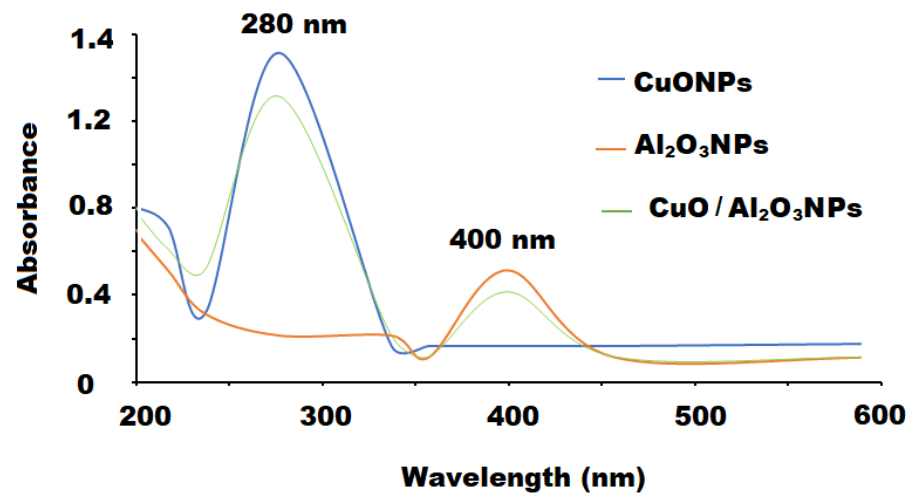


Figure 3. UV-vis spectra of CuONPs ($\lambda_{\max} = 280$ nm), Al_2O_3 NPs ($\lambda_{\max} = 400$ nm) and CuO/ Al_2O_3 nanocomposite measured at absorption wavelength ranged between 200–500 nm.

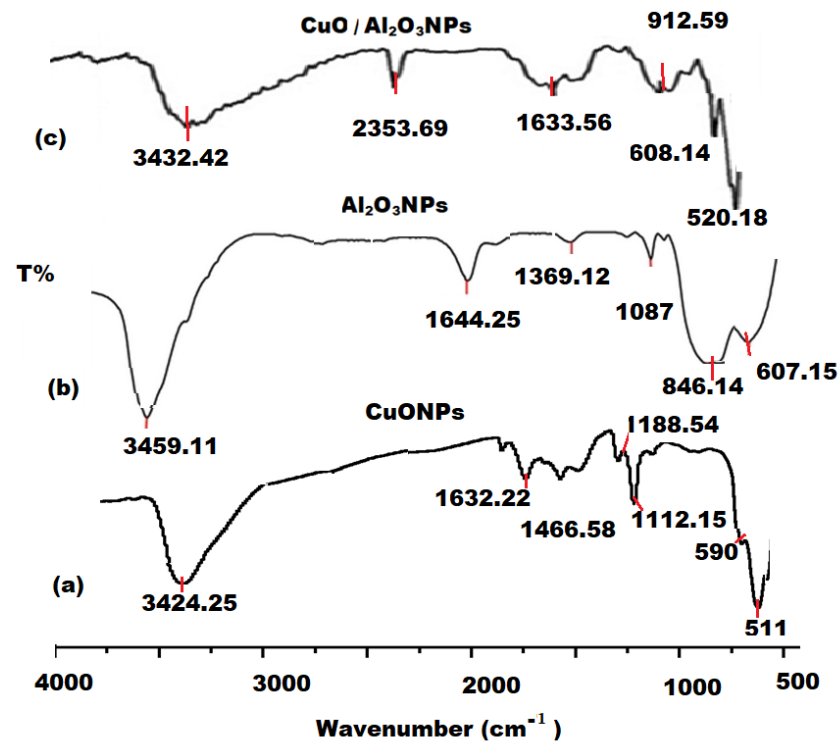


Figure 4. Fourier-Transform Infrared (FT-IR) spectra of the as-synthesized (a) CuONPs, (b) Al_2O_3 NPs and (c) CuO/ Al_2O_3 nanocomposite measured at wavenumber range 4000–500 cm^{-1} .

The XRD analysis were performed to study the crystalline structure of the synthesized CuONPs, Al_2O_3 NPs and CuO/ Al_2O_3 nanocomposite. The XRD pattern of CuONPs showed various characteristic peaks at $2\theta = 32.5^\circ$ (1 1 0), 35.7° (0 0 2), 38.9° (1 1 1), 47.8° (1 1 2), 52.4° (2 0 2), 63.8° (1 1 3), 86.4° (2 2 0), 76.5° (3 1 1) plane orientation of CuO which was verified from the Standard Joint Committee on Powder Diffraction Standards (JCPDS 80-1268). The recorded results from peak positions confirmed the monoclinic structure of the CuONPs and no other phases were noticed, revealing high purity of the formed CuONPs (Figure 5a). The XRD pattern of Al_2O_3 nanoparticles showed that the sample was in nanorods crystalline shape and exhibited different peaks at 32.65° (2 2 0), 35.14° (3 1 1), 37.26° (2 2 2), 43.58° (4 0 0), 54.22° (4 2 2), 59.84° (4 4 0), 74.89° (6 2 0). All observed diffraction peaks can be matched to those of bulk α - Al_2O_3 , with cell

constant ($\alpha = 8.395 \text{ \AA}$), which is in acceptance with the value of (JCPDS file No.10-173). No other impurity phases can be detected, indicating high purity of the synthesized Al_2O_3 nanoparticles (Figure 5b). Very similar diffraction peaks were observed in the XRD pattern of $\text{CuO}/\text{Al}_2\text{O}_3$ nanocomposite. Therefore, the above diffraction peaks can be used to verify the formation of $\text{CuO}/\text{Al}_2\text{O}_3$ nanocomposite (Figure 5c). The prominent peak in the XRD pattern was used to calculate the average crystallite size using a Scherrer formula:

$$D = 0.9\lambda / \beta \cos \theta \quad (3)$$

where λ , θ and β are the X-ray wavelength, Bragg diffraction angle, and the Full width at half maximum of the XRD peak appearing at a diffraction angle θ , respectively. The average crystallite size of the synthesized CuONPs and Al_2O_3 NPs were evaluated to be 17.09 ± 1.1 and 27.61 ± 3.1 nm, respectively.

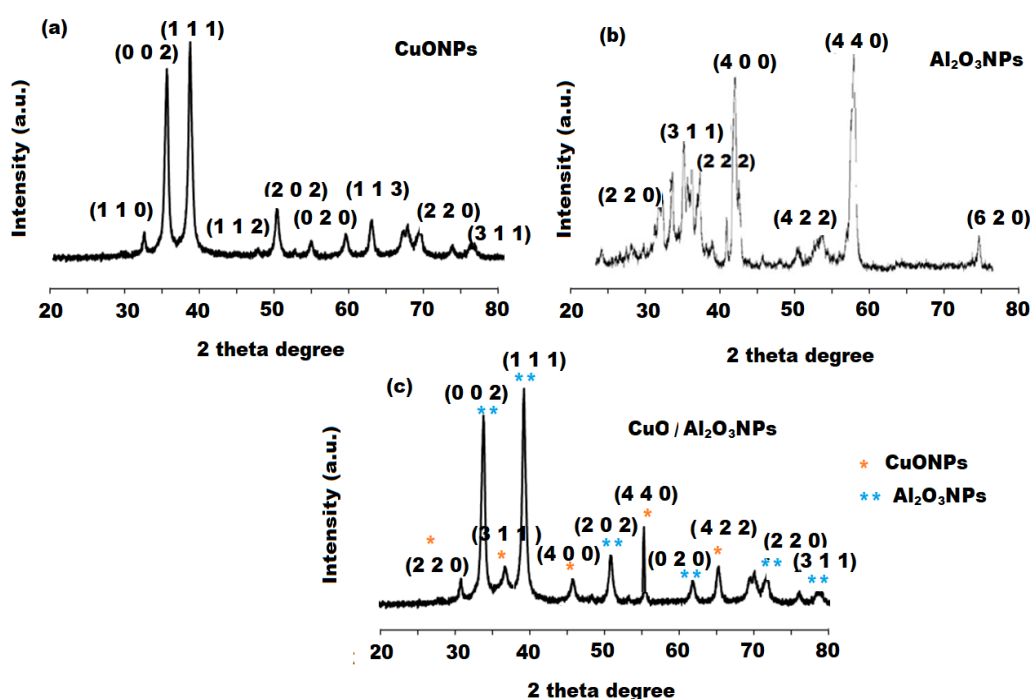


Figure 5. XRD spectra of (a) CuONPs, (b) Al_2O_3 NPs and (c) $\text{CuO}/\text{Al}_2\text{O}_3$ nanocomposite.

The dislocation density (δ), which describes the quantity of defects in the sample is known as the length of dislocation lines per unit volume of the crystal and is calculated using the following equation [54].

$$\delta = 1/D^2 \quad (4)$$

where D is the crystallite size. The dislocation density of CuONPs and Al_2O_3 NPs at room temperature was found to be 1.42×10^{-3} and $1.31 \times 10^{-3} (\text{nm})^{-2}$, respectively.

The bond length of Cu-O and Al-O was calculated from the equation [55].

$$L = \sqrt{\left(\frac{a^2}{3} + \left(\frac{1}{2} - u\right)^2 c^2\right)} \quad (5)$$

where u is the positional parameter in the wurtzite structure and is a measure of the amount by which each atom is displaced according to the next along the 'c' axis. 'u' is given by the equation:

$$u = \frac{a^2}{3c^2} + 0.25 \quad (6)$$

The u value increases with the decreases in c/a ratio this for tetrahedral distances Remaining constant via a distortion of tetrahedral angles. The calculated bond length of

Cu-O and Al-O was found to be 1.928 and 1.869 Å, respectively. The calculated bond length is in agreement with the bond length of Cu-O and Al-O in the unit cell [56,57].

Further microscopic studies were performed using TEM and SEM to confirm the size, shape and surface morphology of CuO/Al₂O₃ nanocomposite according to the as-prepared CuONPs and Al₂O₃NPs. The obtained images of TEM (Figure 6a–c) and SEM (Figure 6d–f) confirmed the uniform distribution of the formed spherical and rod shapes CuONPs and Al₂O₃NPs, respectively. However, the surface morphology of CuO/Al₂O₃ nanocomposite showed highly aggregated crystals with particle sizes ranging from 80–100 nm.

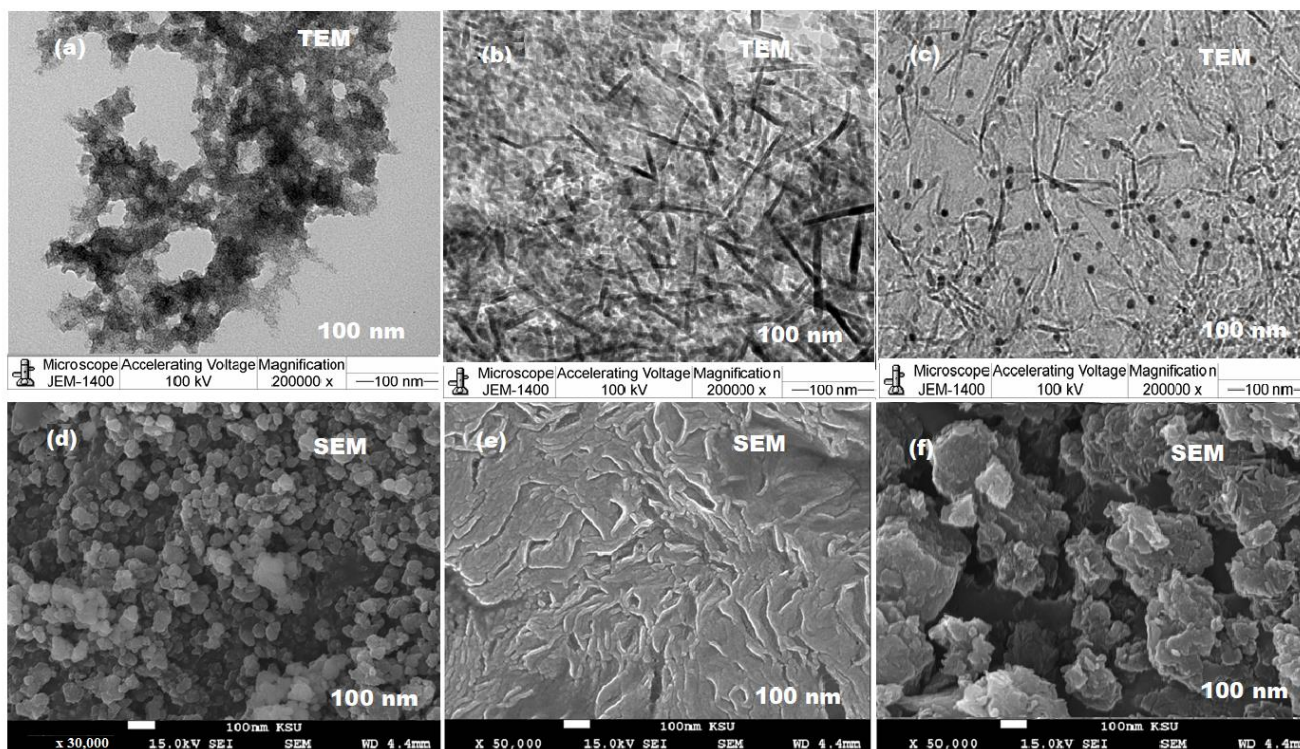


Figure 6. (a–c) TEM and (d–f) SEM images of CuONPs, Al₂O₃NPs and CuO/Al₂O₃ nanocomposite, respectively.

SEM equipped with an EDX spectroscopy was used to evaluate the elemental composition of Cu, Al in the prepared CuO/Al₂O₃ nanocomposite with respect to the EDX profiles of CuONPs and Al₂O₃NPs. The obtained EDX profiles of CuONPs and Al₂O₃NPs showed that the percentage elemental content of Cu, Al, and O was 75.56% (Cu) and 24.44% (O) for CuONPs, 69.88% (Al), and 30.12% (O) for Al₂O₃NPs, with a maximum peak intensity 1.5 and 1.2 keV for Cu and Al, respectively (Figure 7a,b). Whereas the recorded EDX profile of CuO/Al₂O₃ nanocomposite exerts 57.46% Cu, 31.97% Al, and 10.57% O, which suggested the complete reduction of Cu and Al and the high purity of the synthesized CuO/Al₂O₃ nanocomposite (Figure 7c).

3.2. Characteristics of the Constructed Sensors

NTX reacts with TPB to produce a very stable complex NTX-TPB, which is soluble in THF. The conventional NTX-TPB and modified coated wire NTX-TPB-CuO/Al₂O₃NPs nanocomposite sensors were designed by mixing the electroactive materials (ion pairs) with PVC and a solvent mediator (*o*-NPOE) using THF. The current study suggested the use of a high dielectric constant (*o*-NPOE, $\epsilon = 24$) serves as a fluidizer allowing the homogeneous dissolution of the electroactive materials and facilitating its mobility and diffusion through the polymeric matrix of the membrane. Also, it enhances the selectivity coefficient of the sensor by offering a suitable mechanical property for the coated membrane [53]. Table 1 reported the effective potential response and the potentiometric behavior of the constructed NTX-TPB and NTX-TPB-CuO/Al₂O₃NPs nanocomposite sensors. The ob-

tained data showed that the designed sensors exhibited Nernstian behavior with slopes of $E_{mV} = (52.1 \pm 0.2) \log [\text{NTX}] + 406.6$ and $E_{mV} = (58.25 \pm 0.3) \log [\text{NTX}] + 754.25$ with linearity ranges 1.0×10^{-5} – $1.0 \times 10^{-2} \text{ mol L}^{-1}$ ($r^2 = 0.9995$) and 1.0×10^{-9} – $1.0 \times 10^{-2} \text{ mol L}^{-1}$ ($r^2 = 0.9999$) for the above-mentioned sensors, respectively (Figure 8a,b). The addition of CuO/Al₂O₃ nanocomposite to modify the conventional NTX-TPB sensor enhanced the potential response of the designed sensor (NTX-TPB- CuO/Al₂O₃ nanocomposite) to a wider linear detection range with high sensitivity towards the detection of NTX solution. These results can be attributed to the large surface area of the added nanoparticles which increased the surface conductivity of the designed modified sensor. Additionally, the higher detection results observed by using the modified sensor could be due to the high dielectric permittivity value of CuONPs ($\approx 10^4$) and Al₂O₃NPs (≈ 7.8 – 11.1) at ambient temperature [58,59]. The dynamic response of the designed NTX-TPB conventional and modified NTX-TPB-CuO/Al₂O₃NPs nanocomposite sensors were investigated under optimized experimental conditions to detect the difference between the instant potential time and its steady-state value (1 mV) [60]. The recorded dynamic responses were found to be 70 s and 50 s for the above-mentioned conventional and modified sensors, respectively. It was observed that the modified sensor with metal oxide nanocomposite exhibited a fastness response with high mechanical stability more than the conventional type. The modification of the membrane with high surface area to volume ratio metal oxides nanocomposite and new unique physicochemical properties enhances the electrical conductivity of the modified sensor towards the detection of the tested analyte in the sample. Moreover, the remarkable electrical and exceptional capacity characteristics of metal oxides nanocomposite such as the high charge transfer resulting at the nanomaterial interfaces are of paramount importance when the nanomaterials are employed as transducing materials in sensing applications [61].

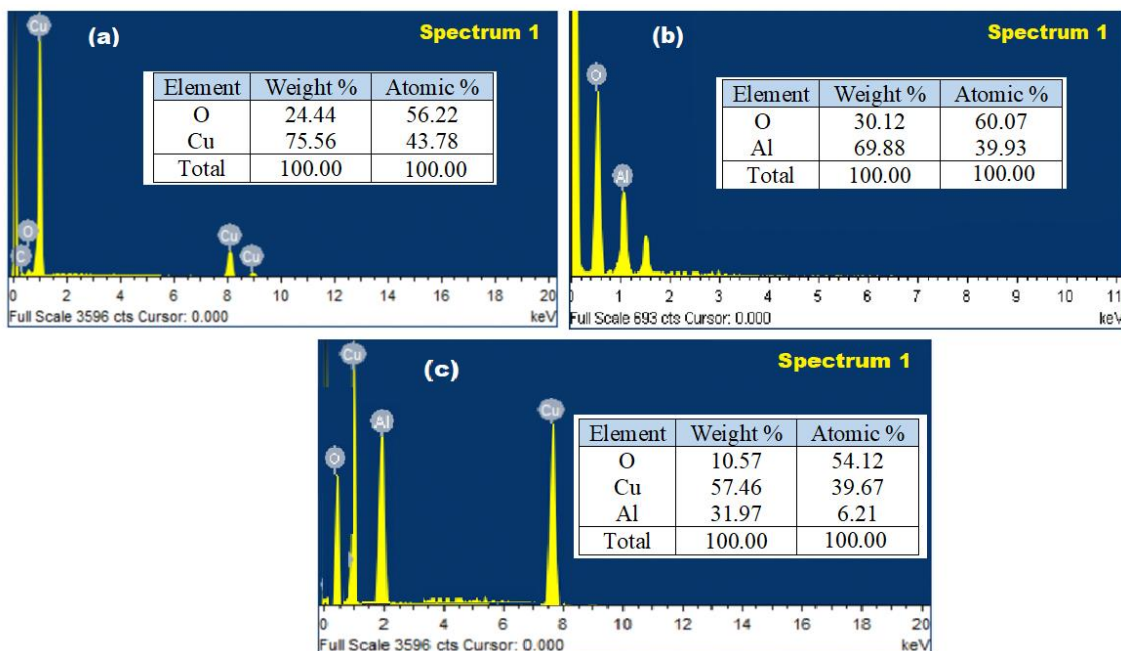
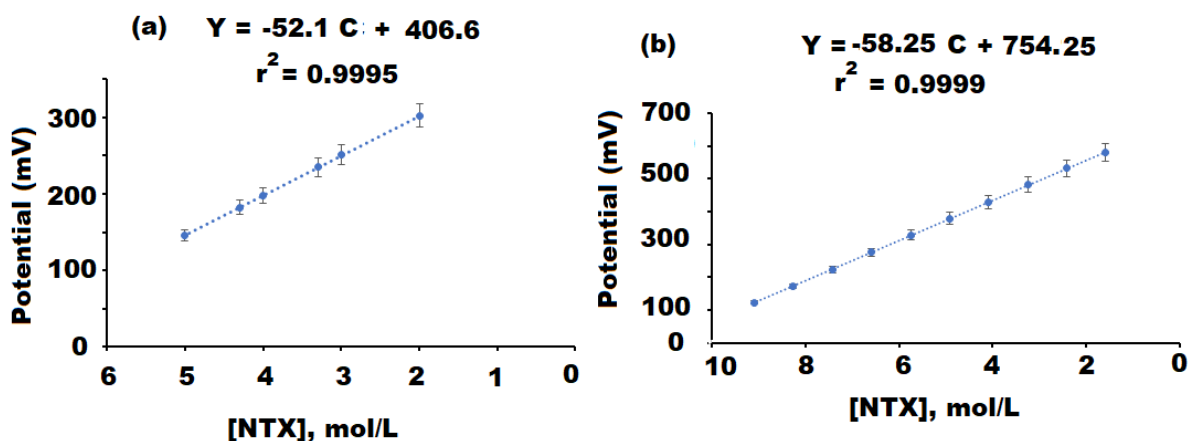


Figure 7. Energy Dispersive X-ray (EDX) analysis of (a) CuONPs, (b) Al₂O₃NPs and (c) CuO/Al₂O₃ nanocomposite.

Table 1. Critical response features of designed conventional coated wire naltrexone -tetraphenyl borate (NTX-TPB) and modified NTX-TPB-CuO/Al₂O₃ nanocomposite sensors.

Parameter	Conventional Coated Wire NTX-TPB Sensor	Modified NTX-TPB-CuO/Al ₂ O ₃ Nanocomposite Sensor
Linear conc. (mol L ⁻¹)	1.0 × 10 ⁻⁶ –1.0 × 10 ⁻²	1.0 × 10 ⁻¹¹ –1.0 × 10 ⁻²
Regression equation	E _{mV} = (52.1 ± 0.2) log [NTX] + 406.6	E _{mV} = (58.25 ± 0.3) log [NTX] + 754.25
Correlation Coefficient (r)	0.9995	0.9999
Slope (mV. Decade ⁻¹)	52.1 ± 0.2	58.25 ± 0.3
Intercept	406.6	754.25
LOD	5.0 × 10 ⁻⁶	5.0 × 10 ⁻¹⁰
Suitable pH range	2–5	2–5
Temperature (°C)	25	25
Lifetime (day)	30	60
Accuracy (%)	98.73 ± 1.09	99.72 ± 0.4
Robustness	98.45 ± 0.7	99.63 ± 0.3
Ruggedness	98.59 ± 0.4	99.68 ± 0.4

**Figure 8.** Linear relationships of (a) Conventional NTX-TPB and (b) NTX-TPB-CuO/Al₂O₃ nanocomposite coated wire sensors.

The hydrogen ion concentration can greatly affect the potential response of the membrane sensor. Thus, it is very necessary to determine the suitable pH range where the potential response of the coated membrane sensor is not affected by hydrogen ions. The obtained results showed that the above-mentioned NTX-TPB and NTX-TPB-CuO/Al₂O₃NPs nanocomposite sensors are independent in the pH range 2–5 and NTX can be simply estimated using the designed sensors within this pH range (Figure 9). It was observed that at high [H⁺] in acidic medium (pH < 2), the protonated ion-pair complex was formed, and the potential readings of the sensors were slightly increased due to the poor responsiveness to NTX ions, whereas at high [OH⁻] in alkaline medium (pH > 5) the potential readings were gradually decreased as a result of a competition between NTX ions and OH⁻ ions and hence reduces the interaction between the investigating drug ions and the sites of ion-pair on the sensor membrane [62].

A separate solution method [50] was applied to evaluate the interference effect of some foreign substances on the selectivity coefficient of the constructed NTX sensors using 1.0 × 10⁻³ mol L⁻¹ solution. The modified NTX-TPB-CuO/Al₂O₃ nanocomposite sensors exhibited excellent selectivity. The unique physicochemical features of the synthesized CuO/Al₂O₃NPs and their large surface area increase the conductivity of the designed modified sensor and hence elevate its selectivity towards the detected NTX ions. Moreover, the NTX coated membrane selectivity is refer to the free energy transfer of ions (NTX⁺) generated between the active sites in the membrane and the working solution. No interferences were noticed by the tested co-additives and amino acids. Thus, excellent selectivity and

good tolerance were accomplished by using the modified NTX sensor for the determination of NTX (Table 2).

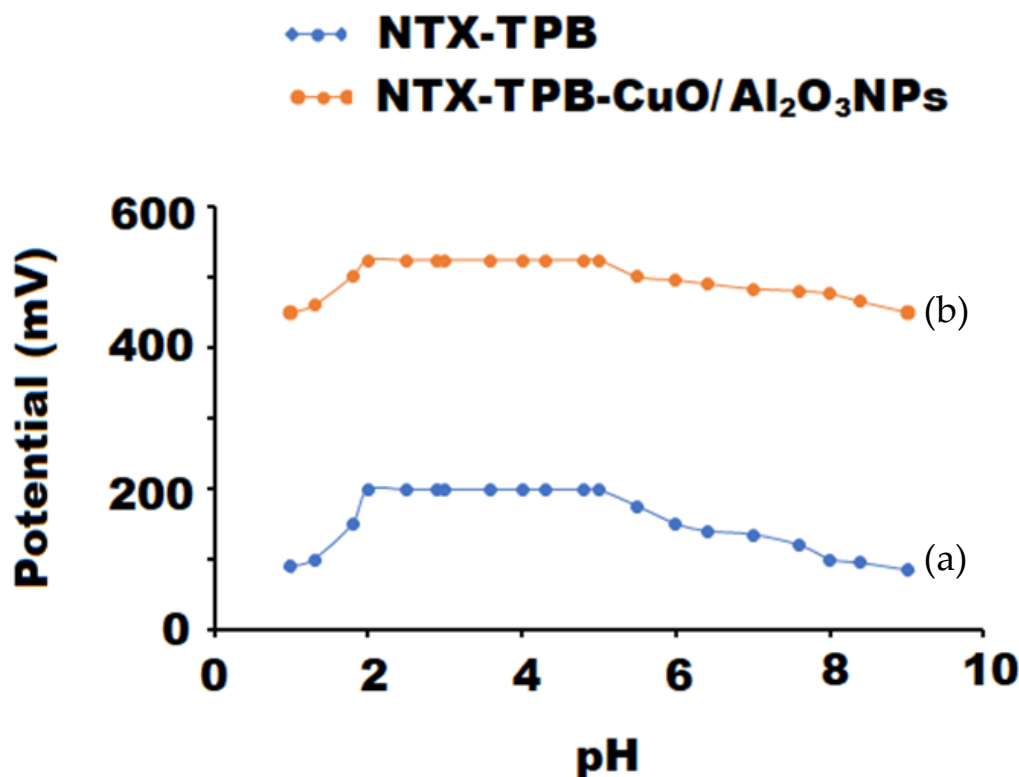


Figure 9. pH range of each constructed Conventional (a) NTX-TPB and (b) NTX-TPB-CuO/Al₂O₃ nanocomposite coated wire sensors using 1.0×10^{-4} mol L⁻¹ of NTX solution.

Table 2. The tolerable values of some foreign substances and co-formulated materials measured by the designed conventional coated wire NTX-TPB and modified NTX-TPB-CuO/Al₂O₃ nanocomposite sensors using separate solution method.

Interferences	Conventional Coated Wire NTX-TPB Sensor ($K^{\text{Pot}}_{\text{NTX}^+}$)	Modified NTX-TPB-CuO/Al ₂ O ₃ Nanocomposite Coated Wire Sensor ($K^{\text{Pot}}_{\text{NTX}^+}$)
Povidone	5.6×10^{-3}	1.5×10^{-5}
Hydroxypropyl methylcellulose	1.9×10^{-3}	5.6×10^{-4}
Lactose monohydrate	4.2×10^{-3}	2.8×10^{-5}
Magnesium stearate	9.4×10^{-3}	3.9×10^{-5}
Microcrystalline cellulose	4.9×10^{-3}	1.7×10^{-4}
Polyethylene glycol	6.3×10^{-3}	3.3×10^{-5}
Polysorbate 80	1.2×10^{-3}	6.9×10^{-5}
Tryptophan	5.6×10^{-3}	2.4×10^{-4}
Lysine	5.3×10^{-3}	5.0×10^{-5}
Glycine	3.3×10^{-3}	3.6×10^{-5}

3.3. Estimation of NTX in Bulk Form

The suggested conventional NTX-TPB and NTX-TPB-CuO/Al₂O₃ sensors were used to estimate NTX in its bulk form and the obtained results were calculated as percentage recoveries of $98.33 \pm 0.9\%$ and $99.81 \pm 0.2\%$ for the above-mentioned sensors, respectively (Table 3). The high dynamic response of the modified sensor can be due to the advanced conductivity and dielectric permittivity properties of the used CuONPs ($\approx 10^4$) and Al₂O₃NPs (≈ 7.8 – 11.1), which provide excellent sensitivity and selectivity towards NTX solution.

Table 3. The calculated resulted of pure NTX estimation using the designed conventional coated wire NTX-TPB and modified NTX-TPB-CuO/Al₂O₃ nanocomposite sensors.

	Conventional Coated Wire NTX-TPB Sensor		Modified NTX-TPB-CuO/Al ₂ O ₃ Nanocomposite Coated Wire Sensor	
	Test Sample −log [NTX] mol L ^{−1}	% Recovery	Test Sample −log [NTX] mol L ^{−1}	% Recovery
Statistical analysis	6.0	99.5	9.0	99.9
	5.3	98.9	8.0	99.6
	5.0	99.0	7.0	100.0
	4.0	97.3	6.0	99.7
	3.0	97.3	5.0	99.6
	2.0	98.0	4.0	100.0
			3.0	99.7
		2.0	100.0	
Mean ± SD	98.33 ± 0.9		99.81 ± 0.2	
n	6		8	
Variance	0.81		0.04	
%SE *	0.37		0.07	
%RSD	0.92		0.20	

* %SE (%Error) = %RSD/√n.

3.4. Validation Study

The International Council for Harmonization of Technical Requirements for Pharmaceuticals (ICH) guidelines [49] were employed to ensure the validity and suitability of the suggested potentiometric method. Linear relationships in the concentration ranges 1.0×10^{-5} – 1.0×10^{-2} and 1.0×10^{-9} – 1.0×10^{-2} mol L^{−1} with least square regression equations $E_{mV} = (52.1 \pm 0.2) \log [\text{NTX}] + 406.6$ ($r^2 = 0.9995$) and $E_{mV} = (58.25 \pm 0.3) \log [\text{NTX}] + 754.25$ ($r^2 = 0.9999$) and low detection limits of 5.0×10^{-6} and 5.0×10^{-10} mol L^{−1} for the conventional and modified NTX sensors, respectively.

The accuracy of the suggested potentiometric method was studied using nine authentic NTX concentrations and the results were expressed as mean percentage recoveries as $98.73 \pm 1.09\%$ and $99.72 \pm 0.4\%$ for NTX-TPB and NTX-TPB-CuO/Al₂O₃ nanocomposite, respectively (Table 4). The precision was also studied using intra-day and inter-day assays. The recorded results were expressed as a percentage relative standard deviation (%RSD) as 0.3% and 0.2% for the two constructed NTX sensors, respectively (Table 5). The system robustness was evaluated by performing a slight variation in method parameter by changing the pH of working solutions to 5 ± 0.5 . The calculated percentage recoveries were $98.45 \pm 0.7\%$ and $99.63 \pm 0.3\%$ for the conventional and modified NTX coated wire sensors (Table 1). Another experiment was carried out to ensure the ruggedness of the suggested potentiometric method by performing the analysis using another pH-meter (Metrohm model-744) in the different laboratories and different operators. The mean percentage recoveries were found to be $98.59 \pm 0.6\%$ and $99.68 \pm 0.4\%$ for the above NTX sensors, respectively (Table 1). The outcomes of method validation revealed a good agreement with those resulting from the suggested method and no remarkable differences was noticed.

3.5. Analysis of NTX in Naltrexone Hydrochloride[®] Tablets

The investigated NTX was determined in its commercial tablets Naltrexone hydrochloride[®] (50 mg/tablet) using the constructed NTX-TPB and NTX-TPB-CuO/Al₂O₃ nanocomposite. The potential readings of the working solutions 1.0×10^{-5} – 1.0×10^{-2} and 1.0×10^{-9} – 1.0×10^{-2} mol L^{−1} were measured and the percentage recoveries of NTX were estimated from the regression equations. The recorded results were calculated as $99.05 \pm 0.5\%$ and $99.70 \pm 0.2\%$ for the above-designed sensors. The obtained results were compared with the reported method by Ganjali et al. [63] using the t-student's test and F-test [64] and showed excellent sensitivity and selectivity of the designed sensor for the

determination of NTX (Table 6). The dielectric constant is a critical factor that evaluate the capability of the materials to store charges [65]. Metal oxides with high dielectric constant are commonly used in electronics and sensors. As they do not permit the flow of charges through them, they allow for exerting electrostatic fields and storing charges [66]. The combination of metal oxides nanoparticles with polymeric matrix in nanocomposites could effectively improve the electrical, optical and conductive properties of the modified sensor. These properties are much sensitive to changes in the particles shape and size. As previously reported the nanoparticles themselves could serve as conductive junctions between the polymeric chains that resulted in as increase of electrical conductance of the composites [67]. Additionally, the modification of the sensor with nanocomposite containing metal oxides with high surface area to volume ratios and possess new physicochemical properties enhanced the charge transfer and the electrical conductivity of the sensor towards the interaction with the target analyte in the test solution and resultingly improve sensitivity of the sensor detection [68].

Table 4. The accuracy study for NTX estimation using the designed conventional coated wire NTX-TPB and modified NTX-TPB-CuO/Al₂O₃ nanocomposite sensors.

	Conventional Coated Wire NTX-TPB Sensor		Modified NTX-TPB-CuO/Al ₂ O ₃ Nanocomposite Coated Wire Sensor	
	Test Sample −log [NTX] mol L ^{−1}	% Recovery	Test Sample −log [NTX] mol L ^{−1}	% Recovery
Statistical Analysis	6.0	99.9	9.0	99.9
	5.3	97.9	8.3	99.7
	5.0	99.5	8.0	99.9
	4.3	98.3	7.0	99.6
	4.0	97.3	6.0	100.0
	3.3	98.9	5.0	99.7
	3.0	99.7	4.0	98.8
	2.3	97.2	3.0	100.0
	2.0	99.9	2.0	99.9
Mean ± SD	98.73 ± 1.09		99.72 ± 0.4	
n	9		9	
Variance	1.18		0.16	
%SE *	0.36		0.13	
%RSD	1.10		0.40	

* %SE (%Error) = %RSD/√n.

A comparative study was carried out to compare the efficiency of the designed modified NTX-TPB-CuO/Al₂O₃ nanocomposite sensor with the previously constructed sensors [63,69,70]. The comparative results revealed high sensitivity of the modified sensor towards the determination of NTX with a wide detection range of 1.0×10^{-9} – 1.0×10^{-2} and LOD 5.0×10^{-6} mol L^{−1} than the reported (Table 7). The selection of nanostructured materials and sensor design method is the most important factor for achieving ultrasensitive sensor with desired characteristics. The shape and size of the nanoparticles used governs the surface to volume ratio, which is a crucial factor to enhance the interface reactions on the overall nanomaterial's electrical conductivity. The nanoscale morphology will not only influence the sensitivity of the sensor but also affect the dynamic response of the sensor and the long-term stability of the sensor due to the high chemical stability of these nanomaterials. The electrical conductivity of the fabricated sensors using metal oxide nanocomposite might also based on the molecular structure and the polymeric medium such as the crystallinity and long chain polymer [71].

Table 5. Intermediate precision assay of the designed modified NTX-TPB-CuO/Al₂O₃ nanocomposite coated wire sensors.

	Modified NTX-TPB-CuO/Al ₂ O ₃ Nanocomposite Coated Wire Sensor					
	Intra-Day Assay			Inter-Day Assay		
	Sample −log [NTX] mol L ^{−1}	Found −log [NTX] mol L ^{−1}	% Recovery	Sample −log [NTX] mol L ^{−1}	Found −log [NTX] mol L ^{−1}	% Recovery
Statistical Analysis	11.0 7.0 2.0	10.99 7.0 1.99	99.9 100.0 99.5	11.0 7.0 2.0	11.0 6.98 2.01	100.0 99.7 100.2
Mean ± SD		99.8 ± 0.3			99.9 ± 0.2	
n		3			3	
Variance		0.09			0.04	
%SE *		0.17			0.11	
%RSD		0.30			0.20	

* %SE (%Error) = %RSD/√n.

Table 6. The calculated resulted from the quantification of NTX in Naltrexone hydrochloride[®] 50 mg/tablet using the designed conventional coated wire NTX-TPB and modified NTX-TPB-CuO/Al₂O₃ nanocomposite sensors.

	Conventional Coated Wire NTX-TPB Sensor		Modified NTX-TPB-CuO/Al ₂ O ₃ Nanocomposite Coated Wire Sensor		Reported Method [63]
	Test Sample −log [NTX] mol L ^{−1}	% Recovery	Test Sample −log [NTX] mol L ^{−1}	% Recovery	
Statistical analysis	6.0	99.8	11.0	100.00	99.52 ± 0.3 6 0.09 0.12 0.30
	5.3	99.6	9.0	99.9	
	5.0	98.8	7.0	99.8	
	4.0	98.5	5.0	99.6	
	3.0	98.7	3.0	99.4	
	2.0	98.9	2.0	99.5	
Mean ± SD	99.05 ± 0.5		99.70 ± 0.2		
n	6		6		
Variance	0.25		0.04		
%SE *	0.20		0.08		
%RSD	0.50		0.20		
t-student test	2.015 (2.228) *		1.248(2.228) *		
F-test	2.77 (5.05) *		2.25(5.05) *		

* Tabulated values of t-student test and F-test at $p < 0.05$ [64].**Table 7.** Comparative study between the suggested modified NTX-TPB-CuO/Al₂O₃ nanocomposite sensor and the previously potentiometric reported method.

No.	Ion-Pair Complex	Concentration Range (mol L ^{−1})	LOD (mol L ^{−1})	Reference
1.	NTX- tetraphenylborate	1.0×10^{-5} – 1.0×10^{-2}	8.0×10^{-6}	[63]
2.	NTX- tetraphenylborate	1.0×10^{-5} – 1.0×10^{-3}	5.0×10^{-6}	[69]

Table 7. Cont.

No.	Ion-Pair Complex	Concentration Range (mol L ⁻¹)	LOD (mol L ⁻¹)	Reference
3.	NTX-tetrakis-4 chlorophenyl borate	5.8×10^{-6} – 1.0×10^{-2}	5.0×10^{-6}	[70]
4.	NTX-tetraphenylbotate-CuO/Al ₂ O ₃ nanocomposite	1.0×10^{-9} – 1.0×10^{-2}	5.0×10^{-10}	Current study

4. Conclusions

The present study has described a successfully designed simple and ultrasensitive modified NTX-TPB-CuO/Al₂O₃ nanocomposite potentiometric sensor for the determination of NTX in authentic powder and commercial formulations. The designed modified sensor exhibited a large surface area to volume ratio which granted excellent sensitivity for the detection of NTX with linear relationships in the concentration ranges 1.0×10^{-5} – 1.0×10^{-2} and 1.0×10^{-9} – 1.0×10^{-2} mol L⁻¹ with least square regression equations $E_{mV} = (52.1 \pm 0.2) \log [\text{NTX}] + 406.6$ ($r^2 = 0.9995$) and $E_{mV} = (58.25 \pm 0.3) \log [\text{NTX}] + 754.25$ ($r^2 = 0.9999$) and low detection limits of 5.0×10^{-6} and 5.0×10^{-10} mol L⁻¹ for the conventional and modified NTX sensors, respectively. Outcomes of the suggested method were evaluated statistically and matched with those of previously addressed sensors. It was noticed that the designed modified NTX-TPB-CuO/Al₂O₃ nanocomposite showed a more extraordinary potential response than the conventional type. Furthermore, covering the surface of the sensor by a modified layer of metal oxide nanocomposite polymeric membrane increased the electroconductivity of this sensor and improved the quantification of the tested drug in its tablets with mean percentage recovery $99.70 \pm 0.2\%$ for the above-modified sensor, revealing high sensitivity and selectivity. Therefore, the use of metal oxide nanocomposite in the construction of polymeric sensors opens up a promising area in developing novel modified potentiometric sensors.

Author Contributions: Visualization and formal analysis, A.M.A.-M.; Methodology and writing—review and editing G.A.E.M.; methodology, validation and writing—original draft, M.F.E.-T. All authors have read and agreed to the published version of the manuscript.

Funding: This research was funded by Researchers Supporting Project in King Saud University and the code number is (RSP-2021/247).

Institutional Review Board Statement: Not applicable.

Informed Consent Statement: Not applicable.

Data Availability Statement: All data resulted from this study was presented in the text.

Acknowledgments: This study was supported by Researchers Supporting Project number (RSP-2021/247), King Saud University, Riyadh, Saudi Arabia.

Conflicts of Interest: The authors declare that no conflict of interest associated with this study.

References

- Hassan, T.; Salam, A.; Khan, A.; Khan, S.U.; Khanzada, H.; Wasim, M.; Khan, M.Q.; Kim, I.S. Functional nanocomposites and their potential applications: A review. *J. Polym. Res.* **2021**, *28*, 36. [CrossRef]
- Gholamali, I.; Yadollahi, M. Bio-nanocomposite Polymer Hydrogels Containing Nanoparticles for Drug Delivery: A Review. *Regen. Eng. Transl. Med.* **2021**, *7*, 129–146. [CrossRef]
- Liu, X.; Gu, Y.; Mi, T.; Zhao, Y.; Wang, X.; Zhang, X. Preparation of superhydrophobic fabric based on the SiO₂@PDFMA nanocomposites by an emulsion graft polymerization and a hot-Pressing process. *ChemistrySelect* **2021**, *6*, 5646–5654. [CrossRef]

4. Joseph, J.E.; Mary, P.R.; Haritha, K.V.; Panwar, D.; Kapoor, M. Soluble and cross-linked aggregated forms of α -galactosidase from *Vigna mungo* immobilized on magnetic nanocomposites: Improved stability and reusability. *Appl. Biochem. Biotechnol.* **2021**, *193*, 238–256. [[CrossRef](#)]
5. Noor, M.; Al Mamun, M.A.; Ullah, A.A.; Matsuda, A.; Kawamura, G.; Hakim, M.A.; Islam, M.F.; Matin, M.A. Physics of $Ce^{3+} \leftrightarrow Ce^{4+}$ electronic transition in phytosynthesized $CeO_2/CePO_4$ nanocomposites and its antibacterial activities. *J. Phys. Chem. Solids* **2021**, *148*, 109751. [[CrossRef](#)]
6. Munonde, T.S.; Nomngongo, P.N. Nanocomposites for electrochemical sensors and their applications on the detection of trace metals in environmental water samples. *Sensors* **2021**, *21*, 131. [[CrossRef](#)] [[PubMed](#)]
7. Al-Hossainy, A.F.; Abdelaal, R.M.; El Sayed, W.N. Novel synthesis, structure characterization, DFT and investigation of the optical properties of cyanine dye/zinc oxide [4-CHMQI/ZnO] C nanocomposite thin film. *J. Mol. Struct.* **2021**, *1224*, 128989. [[CrossRef](#)]
8. Chen, Y.; Chen, X.; Zhang, Y. A comprehensive review on metal-oxide nanocomposites for high-performance lithium-ion battery anodes. *Energy Fuels* **2021**, *35*, 6420–6442. [[CrossRef](#)]
9. Sathishkumar, P.; Li, Z.; Govindan, R.; Jayakumar, R.; Wang, C.; Gu, F.L. Zinc oxide-quercetin nanocomposite as a smart nano-drug delivery system: Molecular-level interaction studies. *Appl. Surf. Sci.* **2021**, *536*, 147741. [[CrossRef](#)]
10. Beyene, A.M.; Moniruzzaman, M.; Karthikeyan, A.; Min, T. Curcumin nanoformulations with metal oxide nanomaterials for biomedical applications. *Nanomaterials* **2021**, *11*, 460. [[CrossRef](#)]
11. Shamsazar, A.; Asadi, A.; Seifzadeh, D.; Mahdavi, M. A novel and highly sensitive sandwich-type immunosensor for prostate-specific antigen detection based on MWCNTs-Fe₃O₄ nanocomposite. *Sens. Actuators B Chem.* **2021**, *346*, 130459. [[CrossRef](#)]
12. Ali, M.; Ijaz, M.; Ikram, M.; Ul-Hamid, A.; Avais, M.; Anjum, A.A. Biogenic synthesis, characterization and antibacterial potential evaluation of copper oxide nanoparticles against *Escherichia coli*. *Nanoscale Res. Lett.* **2021**, *16*, 148. [[CrossRef](#)]
13. Benhammada, A.; Trache, D.; Chelouche, S.; Mezroua, A. Catalytic effect of green CuO nanoparticles on the thermal decomposition kinetics of ammonium perchlorate. *Z. Anorg. Allg. Chem.* **2021**, *647*, 312–325. [[CrossRef](#)]
14. Peighambardoust, S.J.; Peighambardoust, S.H.; Pournasir, N.; Pakdel, P.M. Properties of active starch-based films incorporating a combination of Ag, ZnO and CuO nanoparticles for potential use in food packaging applications. *Food Packag. Shelf Life* **2019**, *22*, 100420. [[CrossRef](#)]
15. Yang, L.; Yang, J.; Dong, Q.; Zhou, F.; Wang, Q.; Wang, Z.; Huang, K.; Yu, H.; Xiong, X. One-step synthesis of CuO nanoparticles based on flame synthesis: As a highly effective non-enzymatic sensor for glucose, hydrogen peroxide and formaldehyde. *J. Electroanal. Chem.* **2021**, *881*, 114965. [[CrossRef](#)]
16. Fakhree, F.M.; Waheed, I.F.; Mahmoud, K.M. Synthesis and characterization of CuO nanoparticles stabilized by quercetin and its application for anti-breast cancer activity. *Egypt. J. Chem.* **2021**, *64*, 22–23. [[CrossRef](#)]
17. Resan, S.A.; Essa, A.F. Preparation and study of the optical properties for polyaniline-Al₂O₃ nanocomposite. *Mater. Today Proc.* **2021**, *45*, 5819–5822. [[CrossRef](#)]
18. Zulkifli, F.W.A.; Yazid, H.; Jani, A.M.M. Immobilization of carbon nanotubes decorated gold nanoparticles on anodized aluminium oxide (Au-CNTs-AAO) membrane for enhanced catalytic performance. *Mater. Chem. Phys.* **2021**, *264*, 124445. [[CrossRef](#)]
19. Li, Z.; Wray, P.R.; Su, M.P.; Tu, Q.; Andaraarachchi, H.P.; Jeong, Y.J.; Atwater, H.A.; Kortshagen, U.R. Aluminum oxide nanoparticle films deposited from a nonthermal plasma: Synthesis, characterization, and crystallization. *ACS Omega* **2020**, *5*, 24754–24761. [[CrossRef](#)]
20. Khan, S.; Shah, S.S.; Anjum, M.A.R.; Khan, M.R.; Janjua, N.K. Electro-oxidation of ammonia over copper oxide impregnated γ -Al₂O₃ nanocatalysts. *Coatings* **2021**, *11*, 313. [[CrossRef](#)]
21. Sankar, S.; Parvathi, K.; Ramesan, M.T. Structural characterization, electrical properties and gas sensing applications of polypyrrole/Cu-Al₂O₃ hybrid nanocomposites. *High Perform. Polym.* **2020**, *32*, 719–728. [[CrossRef](#)]
22. Baratto, C.; Kumar, R.; Faglia, G.; Vojisavljevic, K.; Malic, B. p-Type copper aluminum oxide thin films for gas-sensing applications. *Sens. Actuators B Chem.* **2015**, *209*, 287–296. [[CrossRef](#)]
23. Chiang, C.Y.; Aroh, K.; Ehrman, S.H. Copper oxide nanoparticle made by flame spray pyrolysis for photoelectrochemical water splitting—Part I. CuO nanoparticle preparation. *Int. J. Hyd. Energy* **2012**, *37*, 4871–4879. [[CrossRef](#)]
24. Salem, S.; Salem, A.; Parni, M.H.; Jafarizad, A. Microwave-assisted pyrolysis of organometallic gel prepared through ternary combination of surfactants for fabrication of nano-porous gamma alumina: Adsorptive properties, characterization. *J. Chem. Technol. Biotechnol.* **2021**, *96*, 1187–1196. [[CrossRef](#)]
25. Lillo-Ramiro, J.; Guerrero-Villalba, J.M.; Mota-Gonzalez, M.D.L.; Aguirre-Tostado, F.S.; Gutierrez-Heredia, G.; Mejia-Silva, I.; Carrillo-Castillo, A. Optical and microstructural characteristics of CuO thin films by sol gel process and introducing in non-enzymatic glucose biosensor applications. *Optik* **2021**, *229*, 166238. [[CrossRef](#)]
26. Rutkowska, I.; Marchewka, J.; Jelen, P.; Odziomek, M.; Korpys, M.; Paczkowska, J.; Sitarz, M. Chemical and structural characterization of amorphous and crystalline alumina obtained by alternative sol-gel preparation routes. *Materials* **2021**, *14*, 1761. [[CrossRef](#)]
27. Peng, W.; Zhou, Y.; Li, J.; Liu, Y.; Zhang, J.; Xiang, G.; Zhu, X.; Li, R.; Wang, H.; Zhao, Y. Annealing temperature induced physical characteristics of CuO films grown by magnetron sputtering. *Mater. Sci. Semicond. Process.* **2021**, *131*, 105883. [[CrossRef](#)]
28. Ma, C.; Zhao, C.; Fan, X.; Liu, Z.; Liu, J. Preparation of non-stoichiometric Al₂O₃ film with broadband antireflective by magnetron sputtering. *Chem. Phys. Lett.* **2021**, *764*, 138299. [[CrossRef](#)]

29. Menazea, A.A.; Ahmed, M.K. Silver and copper oxide nanoparticles-decorated graphene oxide via pulsed laser ablation technique: Preparation, characterization, and photoactivated antibacterial activity. *Nano-Struct Nano-Objects* **2020**, *22*, 100464. [[CrossRef](#)]
30. ElFaham, M.M.; Okil, M.; Mostafa, A.M. Effects of post-laser irradiation on the optical and structure properties of Al₂O₃ nanoparticles produced by laser ablation. *J. Appl. Phys.* **2020**, *128*, 153104. [[CrossRef](#)]
31. Jadhav, S.; Gaikwad, S.; Nimse, M.; Rajbhoj, A. Copper oxide nanoparticles: Synthesis, characterization and their antibacterial activity. *J. Clust. Sci.* **2011**, *22*, 121–129. [[CrossRef](#)]
32. Merati, Z.; Parsa, J.B.; Babaei-Sati, R. Electrochemically synthesized polypyrrole/MWCNTs-Al₂O₃ ternary nanocomposites supported Pt nanoparticles toward methanol oxidation. *Int. J. Hydrog. Energy* **2018**, *43*, 20993–21005. [[CrossRef](#)]
33. Sodeifian, G.; Behnood, R. Application of microwave irradiation in preparation and characterization of CuO/Al₂O₃ nanocomposite for removing MB dye from aqueous solution. *J. Photochem. Photobiol. A Chem.* **2017**, *342*, 25–34. [[CrossRef](#)]
34. Sudha, V.; Murugadoss, G.; Thangamuthu, R. Structural and morphological tuning of Cu-based metal oxide nanoparticles by a facile chemical method and highly electrochemical sensing of sulphite. *Sci. Rep.* **2021**, *11*, 3413. [[CrossRef](#)]
35. Zhou, X.; Pu, H.; Sun, D.W. DNA functionalized metal and metal oxide nanoparticles: Principles and recent advances in food safety detection. *Crit. Rev. Food Sci. Nutr.* **2021**, *61*, 2277–2296. [[CrossRef](#)] [[PubMed](#)]
36. Dong, Q.; Ryu, H.; Lei, Y. Metal oxide based non-enzymatic electrochemical sensors for glucose detection. *Electrochim. Acta* **2021**, *370*, 137744. [[CrossRef](#)]
37. Pragathiswaran, C.; Thulasi, G.; Al-Ansari, M.M.; Al-Humaid, L.A.; Saravanan, M. Experimental investigation and electrochemical characterization of titanium coated nanocomposite materials for biomedical applications. *J. Mol. Struct.* **2021**, *1231*, 129932. [[CrossRef](#)]
38. Shawky, A.M.; El-Tohamy, M.F. Highly functionalized modified metal oxides polymeric sensors for potentiometric determination of letrozole in commercial oral tablets and biosamples. *Polymers* **2021**, *13*, 1384. [[CrossRef](#)] [[PubMed](#)]
39. Liu, Y.; Liu, Y.; Yan, R.; Gao, Y.; Wang, P. Bimetallic AuCu nanoparticles coupled with multi-walled carbon nanotubes as ion-to-electron transducers in solid-contact potentiometric sensors. *Electrochim. Acta* **2020**, *331*, 135370. [[CrossRef](#)]
40. Dakshayini, B.S.; Reddy, K.R.; Mishra, A.; Shetti, N.P.; Malode, S.J.; Basu, S.; Naveen, S.; Raghu, A.V. Role of conducting polymer and metal oxide-based hybrids for applications in amperometric sensors and biosensors. *Microchem. J.* **2019**, *147*, 7–24. [[CrossRef](#)]
41. Colozza, N.; Tazzioli, S.; Sassolini, A.; Agosta, L.; di Monte, M.G.; Hermansson, K.; Arduini, F. Multiparametric analysis by paper-assisted potentiometric sensors for diagnostic and monitoring of reinforced concrete structures. *Sens. Actuators B Chem.* **2021**, *345*, 130352. [[CrossRef](#)]
42. Al-Tamimi, S.A. Biogenic green synthesis of metal oxide nanoparticles using oat biomass for ultrasensitive modified polymeric sensors. *Green Chem. Lett. Rev.* **2021**, *14*, 166–179. [[CrossRef](#)]
43. Elashery, S.E.; Frag, E.Y.; Sleim, A.A. Novel and selective potentiometric sensors for Cinchocaine HCl determination in its pure and Co-formulated dosage form: A comparative study of in situ carbon sensors based on different ion pairing agents. *Measurement* **2021**, *173*, 108549. [[CrossRef](#)]
44. Nunes, E.V., Jr.; Scodes, J.M.; Pavlicova, M.; Lee, J.D.; Novo, P.; Campbell, A.N.; Rotrosen, J. Sublingual buprenorphine-naloxone compared with injection naltrexone for opioid use disorder: Potential utility of patient characteristics in guiding choice of treatment. *Am. J. Psych.* **2021**, *178*, 660–671. [[CrossRef](#)] [[PubMed](#)]
45. El-Didamony, A.M.; Hassan, W.S. Spectrophotometric and fluorimetric methods for determination of naltrexone in urine, serum and tablets by oxidation with cerium (IV). *J. Chil. Chem. Soc.* **2012**, *57*, 1404–1408. [[CrossRef](#)]
46. Jafari-Nodoushan, M.; Barzin, J.; Mobedi, H. A stability-indicating HPLC method for simultaneous determination of morphine and naltrexone. *J. Chromatogr. B* **2016**, *1011*, 163–170. [[CrossRef](#)] [[PubMed](#)]
47. Abdel-Gawad, S.A.; El-Gamal, R.M. Simultaneous determination of naltrexone and bupropion in their co-formulated tablet utilizing green chromatographic approach with application to human urine. *Saudi Pharm. J.* **2018**, *26*, 169–176. [[CrossRef](#)]
48. Ghorbani-Bidkorbeh, F.; Shahrokhian, S.; Mohammadi, A.; Dinarvand, R. Electrochemical determination of naltrexone on the surface of glassy carbon electrode modified with Nafion-doped carbon nanoparticles: Application to determinations in pharmaceutical and clinical preparations. *J. Electroanal. Chem.* **2010**, *638*, 212–217. [[CrossRef](#)]
49. Draz, M.E.; Darwish, H.W.; Darwish, I.A.; Saad, A.S. Solid-state potentiometric sensor for the rapid assay of the biologically active biogenic amine (tyramine) as a marker of food spoilage. *Food Chem.* **2021**, *346*, 128911. [[CrossRef](#)] [[PubMed](#)]
50. FDA. ICH-Q2 (R1) Validation and Analytical Procedures: Text and Methodology. In Proceedings of the International Conference on Harmonization Guidelines, Geneva, Switzerland, 17 November 2005.
51. Sagadevan, S.; Pal, K.; Chowdhury, Z.Z. Fabrication of CuO nanoparticles for structural, optical and dielectric analysis using chemical precipitation method. *J. Mater. Sci. Mater. Electron.* **2017**, *28*, 12591–12597. [[CrossRef](#)]
52. Abdollahifar, M.; Zamani, R.M.; Beiygie, E.; Nekouei, H. Synthesis of micro-mesopores flowerlike γ -Al₂O₃ nano-architectures. *J. Serbian Chem. Soc.* **2014**, *79*, 1007–1017. [[CrossRef](#)]
53. Rao, K.V.; Smakula, A. Dielectric properties of cobalt oxide, nickel oxide, and their mixed crystals. *J. Appl. Phys.* **1965**, *36*, 2031–2038. [[CrossRef](#)]
54. Saleem, M.; Fang, L.; Ruan, H.B.; Wu, F.; Huang, Q.L.; Xu, C.L.; Kong, C.Y. Effect of zinc acetate concentration on the structural and optical properties of ZnO thin films deposited by Sol-Gel method. *Int. J. Phys. Sci.* **2012**, *7*, 2971–2979. [[CrossRef](#)]
55. Bindu, P.; Thomas, S. Estimation of lattice strain in ZnO nanoparticles: X-ray peak profile analysis. *J. Theor. Appl. Phys.* **2014**, *8*, 123–134. [[CrossRef](#)]

56. Koblova, E.; Ustinov, A.Y.; Shcheka, O. Theoretical study of copper (II) oxide clusters and their interaction with CO. *Appl. Mech. Mater.* **2015**, *709*, 358–363. [[CrossRef](#)]
57. Kubicki, J.D.; Apitz, S.E. Molecular cluster models of aluminum oxide and aluminum hydroxide surfaces. *Am. Mineral.* **1998**, *83*, 1054–1066. [[CrossRef](#)]
58. Bitra, H.C.R.; Rao, A.V.; Babu, K.S.; Rao, G.N. Synthesis and enhanced dielectric properties of copper oxidenanoparticles. *Mat. Chem. Phys.* **2020**, *254*, 123379. [[CrossRef](#)]
59. Yadav, N.; Dabrowski, R.; Dhar, R. Effect of alumina nanoparticles on dielectric permittivity, electrical conductivity, director relaxation frequency, threshold and switching voltages of a nematic liquid crystalline material. *Liq. Cryst.* **2014**, *41*, 1803–1810. [[CrossRef](#)]
60. Kakhkiz, R.M. Application of nanoparticles in the potentiometric ion selective electrodes. *Russ. J. Electrochem.* **2013**, *49*, 458–465. [[CrossRef](#)]
61. Isa, I.M.; Sohaimi, N.M.; Hashim, N.; Kamari, A.; Mohamed, A.; Ahmad, M.; Ghani, S.A. Determination of salicylate ion by potentiometric membrane electrode based on zinc aluminium layered double hydroxides-4(2,4-dichlorophenoxy) butyrate nanocomposites. *Int. J. Electrochem. Sci.* **2013**, *8*, 2112–2121.
62. Ma, T.S.; Hassan, S.S. *Organic Analysis Using Ion Selective Electrodes*; Academic Press: London, UK, 1982; Volume 1–2.
63. Ganjali, M.R.; Alipour, A.; Riahi, S.; Norouzi, P. Design and construction of a naltrexone selective sensor based on computational study for application in pharmaceutical analysis. *Int. J. Electrochem. Sci.* **2009**, *4*, 1153–1166.
64. Miller, J.C.; Miller, J.N. *Statistics for Analytical Chemistry*, 3rd ed.; Ellis Horwood PTR Prentice Hall: New York, NY, USA, 1993.
65. Huang, X.; Jiang, P. Core-shell structured high-k polymer nanocomposites for energy storage and dielectric applications. *Adv. Mater.* **2015**, *27*, 546–554. [[CrossRef](#)] [[PubMed](#)]
66. Robertson, J.; Wallace, R.M. High-K materials and metal gates for CMOS applications. *Mater. Sci. Eng. R Rep.* **2015**, *88*, 1–41. [[CrossRef](#)]
67. Lange, U.; Roznyatovskaya, N.V.; Mirsky, V.M. Conducting polymers in chemical sensors and arrays. *Anal. Chim. Acta* **2008**, *614*, 1–26. [[CrossRef](#)]
68. Prakash, S.; Chakrabarty, T.; Singh, A.K.; Shahi, V.K. Polymer thin films embedded with metal nanoparticles for electrochemical biosensors applications. *Biosen. Bioelectron.* **2013**, *41*, 43–53. [[CrossRef](#)] [[PubMed](#)]
69. Ghorbani-Bidkorbeh, F.; Shahrokhian, S.; Mohammadi, A.; Dinarvand, R. Preparation of a naltrexone HCl potentiometric sensor and its application to pharmaceutical analysis and drug determination in biological fluids. *J. Food Drug Anal.* **2011**, *19*, e51. [[CrossRef](#)]
70. AlRabiah, H.; Abounassif, M.; Al-Majed, A.; Mostafa, G. Comparative investigation of β - and γ -cyclodextrin as ionophores in potentiometric based sensors for naltrexone. *Int. J. Electrochem. Sci.* **2016**, *11*, 4930–4942. [[CrossRef](#)]
71. Steinhauer, S. Gas Sensors Based on Copper Oxide Nanomaterials: A Review. *Chemosensors* **2021**, *9*, 51. [[CrossRef](#)]